NASA Contractor Report 4203

Hierarchic Plate and Shell Models Based on p-Extension

Barna A. Szabó and Glenn J. Sahrmann
Washington University
St. Louis, Missouri

Prepared for
Langley Research Center
under Grant NAG1-639

National Aeronautics
and Space Administration

**Scientific and Technical
Information Division**

1988

TABLE OF CONTENTS

1. INTRODUCTION.

Assurance of the reliability and accuracy of computed data is fundamentally important in computer aided analysis and design. In this paper we address the question of how to ensure the reliability and accuracy of computed data in engineering computations concerned with analyses of structures comprised of beam, arch, plate and shell components and components which require fully three dimensional representation. We consider only formulations based on the linear theory of elasticity but our approach can be generalized to cases that involve geometric and/or material nonlinearities.

Beams and arches are three dimensional bodies characterized by the fact that two of the three dimensions are much smaller than the third. Similarly, plates and shells are three dimensional bodies characterized by the fact that one of the dimensions is much smaller than the other two. The various theories for beams, arches, plates and shells recognize and exploit this. These theories are useful because the quantities of interest in the analyses of beams, arches, plates and shells, such as membrane forces, bending moments and shear forces, are related to certain averages of the displacement across the small dimension(s) of these three dimensional bodies. This permits reduction of the dimensions in the case of beams and arches from three to one and in the case of plates and shells from three to two.

In engineering problems the line of demarkation between problems of three dimensional elasticity and problems which can be modeled with conventional beam, arch, plate and shell theories is not sharp. Usually plates and shells are stiffened and/or joined with solid bodies. Of greatest engineering interest are the neighborhoods of shell intersections, cutouts, attachments, etc. where the stress states are truly three dimensional and therefore the assumptions of conventional shell theories do not hold. If we are to ensure the reliability and accuracy of computed data without sacrificing computational efficency then we must be able to model these parts of the structure with three dimensional theories while retaining the simplifying assumptions incorporated in plate and shell theories where those assumptions

hold. This raises the fundamentally important question stated by Naghdi in [1] as follows:

> *"Under what circumstances do the equations of shell theory supply an approximate solution to the three-dimensional equations and how 'close' is this approximate solution to the exact solution?"*

In this paper we present a systematic process which provides means for finding answers to this question with respect to specific problems in engineering design and analysis. Our approach is based on *hierarchic* sequences of approximation constructed in such a way that the approximate solutions corresponding to a hierarchic sequence of models converge to the exact solution of the fully three dimensional model. Selection of the discretization parameters and the stopping criterion are based on (1) estimation of the relative error in energy norm; (2) equilibrium tests, and (3) observation of the convergence of quantities of interest. This approach is closely related to p-extension procedures which have been used successfully for estimating and controlling errors of discretization.

Several beam, arch, plate and shell theories exist. These theories have been created and justified by two approaches:

(a) By a priori assumptions concerning the mode of deformation. This approach is favored in the engineering literature, see for example [2-4].

(b) By power series expansion of the solution of the three dimensional differential equations of elasticity so that powers of the thickness parameter are factored. There are several possible variants of this approach: The power series expansion can be applied to the differential equations of elasticity directly (see for example [5-8]) or any of the variational formulations of the differential equations of elasticity. Power series expansion procedures applied to variational formulations lead to theories characterized by the variational formulation. Ciarlet and Destuynder showed, without a priori assumptions based on physical arguments, that Kirchhoff's theory of plates is the first in a sequence of plate theories that can be constructed from the Hellinger-Reissner variational principle [9].

In this paper we will be concerned with formulations based on the principle of virtual work or, equivalently, the principle of minimum potential energy. Our

focus is not on the development or justification of new theories for beams, arches, plates or shells but on aspects of computer implementation of hierarchic sequences of finite element spaces suitable for numerical treatment of a large variety of practical problems which may concurrently contain thin and thick plates and shells, stiffeners, and regions where truly three dimensional representation is required. The discretization parameters which characterize the transverse variation of the displacement components are not fixed a priori, but taken into consideration in the selection of discretization.

We have selected the principle of virtual work as the basis for our formulation because this is the best understood formulation among alternatives and we have substantial experience with it. Analogous construction of hierarchic approximation spaces is possible for formulations based on other principles.

Error control procedures require feedback information concerning the accuracy of the solution in terms of the quantities of interest, and means for reducing the error when necessary. Our approach makes it possible to select sequences of discretization by adaptive or feedback procedures. We will outline and demonstrate such procedures by examples.

2. CONVENTIONAL AND HIERARCHIC THEORIES FOR PLATES AND SHELLS

We note that there are fundamental differences between the motivations underlying the development of classical and modern approaches to modeling of plates and shells. Development of classical theories was motivated by the recognition that the system of partial differential equations of three dimensional elasticity is intractable analytically except in severely restricted cases. Reduction of the number of dimensions in the case of beams, arches and bars from three to one and in the case of plates and shells from three to two permit analytical treatment of large classes of problems. In the cases of arches and shells the coordinate systems must be appropriately chosen (e.g. cylindrical, spherical, ellipsoidal, etc. systems) to allow analytical treatment. Comprehensive surveys of classical theories with historical notes and lists of key references are available in [1,10].

The motivation of modern development is quite different. The main goal is to allow computer implementation so that a very wide range of problems can be analyzed by numerical methods efficiently and with guarantee of reliability. The range of problems is to include, for example, simple bars as well as laminated shells of arbitrary curvature, regions of shell intersections and solid bodies attached to shells.

In the following we briefly review the essential features of the most widely used conventional plate and shell theories and outline the hierarchic theory. The notation used for representing the components of the displacement vector $\vec{u}$ is given in Fig. 2.1.

2.1 Kirchhoff's theory.

In Kirchhoff's theory of plates, formulated in 1850 [11], there are three displacement fields. The functions $u_{x0}(x,y)$, $u_{y0}(x,y)$ in the following equations represent the components of the in-plane displacement vector in the x and y directions, respectively, and the function $u_{z0}(x,y)$ represents the transverse displacement vector component.

$$u_x = u_{x0}(x,y) - z\,\frac{\partial u_{z0}}{\partial x} \tag{2.1a}$$

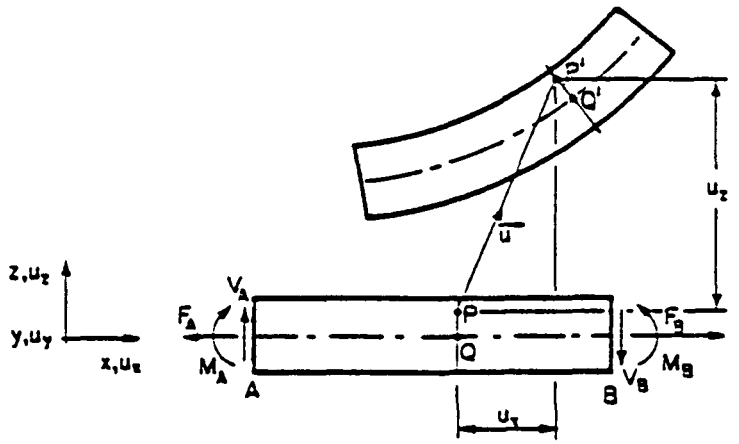

Fig. 2.1. Components of the displacement vector. Notation.

$$u_y = u_{y0}(x,y) - z\,\frac{\partial u_{z0}}{\partial y} \tag{2.1b}$$

$$u_z = u_{z0}(x,y). \tag{2.1c}$$

In its generalization to shells, known the Kirchhoff-Love theory [12], u_x, u_y, u_z are understood to mean the curvilinear (contravariant) displacement components.

From the assumed mode of deformation: $\epsilon_z \stackrel{\text{def}}{=} \partial u_z/\partial z = 0$. The assumption that $\sigma_z = 0$ implies that the plate is orthotropic with Poisson's ratios $\nu_{xz} = \nu_{yz} = 0$. The shear strains γ_{xz} and γ_{yz} are zero. E.g.:

$$\gamma_{xz} \stackrel{\text{def}}{=} \frac{\partial u_x}{\partial z} + \frac{\partial u_z}{\partial x} = -\frac{\partial u_{z0}}{\partial x} + \frac{\partial u_{z0}}{\partial x} = 0.$$

In applications of the principle of virtual work the transverse displacement u_{z0} and its first derivatives must be continuous. This is a major disadvantage of this formulation because enforcement of slope continuity is difficult in the general case.

2.2. The Reissner-Mindlin theory.

In the Reissner-Mindlin theory, formulated in the 1940's and early 1950's [13-15], two new fields u_{x1}, u_{y1}, are introduced. These fields represent the rotation of the cross-sectional planes to which (respectively) the x-axis and y-axis is normal:

$$u_x = u_{x0}(x,y) - z u_{x1}(x,y) \tag{2.2a}$$

$$u_y = u_{y0}(x,y) - z u_{y1}(x,y) \tag{2.2b}$$

$$u_z = u_{z0}(x,y) \tag{2.2c}$$

Again, $\epsilon_z = 0$ and $\sigma_z = 0$ is assumed. The shear strains γ_{xz} and γ_{yz} are independent of z. For example:

$$\gamma_{xz} = -u_{x1}(x,y) + \frac{\partial u_{z0}}{\partial x}$$

In applications of the principle of virtual work the shear strain energy is adjusted by a *shear factor*. In its generalization to shells u_x, u_y, u_z are understood to mean the curvilinear (contravariant) displacement components [16].

2.3. Higher order theories.

In higher order theories the displacement fields are typically approximated by expressions of the form:

$$u_x = \sum_{i=0}^{n} f_i(z)\, u_{xi}(x,y) \tag{2.3a}$$

$$u_y = \sum_{i=0}^{n} f_i(z)\, u_{yi}(x,y) \tag{2.3b}$$

$$u_z = \sum_{i=0}^{m} f_i(z)\, u_{zi}(x,y). \tag{2.3c}$$

Usually $f_i(z) = z^i$. The various theories differ in the chice of n and m and the constitutive law. For example, in the plate theory proposed by Lo, Christensen and Wu [17,18] $n = 3$, $m = 2$ and the constitutive law is the stress-strain law of isotropic elasticity. Discussion of other higher order theories is available in [17].

2.4. Hierarchic theories.

A hierarchic theory is essentially a system of progressively higher order theories based on the same generalized formulation and the same constitutive law. Each theory within a hierarchic system is embedded in all higher order theories in that system and the approximate solutions corresponding to progressively higher order theories converge to the exact solution of the generalized formulation of the fully three dimensional problem. Various hierarchic theories can be constructed by choosing alternative generalized formulations, e.g. the Hellinger-Reissner principle, the principle of virtual work, etc.

In this paper we present a hierarchic system of theories based on the principle of virtual work for homogeneous plates. The general form of approximation is the

same as in (2.3a,b,c). We propose hierarchic basis functions for the displacement components $u_{xi}(x,y)$, $u_{yi}(x,y)$, $u_{zi}(x,y)$ so that shell elements can be readily joined with three dimensional finite elements. The formulation can be extended to apply to laminated plates and shells as well. This is briefly discussed in Section 3.3.

3. HIERARCHIC BEAM, ARCH, PLATE AND SHELL MODELS.

In this section the procedures for the computation of stiffness matrices and load vectors for hierarchic plate and shell models are described. We begin with the simplest representative case for this class of problems, the case of beam-columns and arches.

3.1. Beam-columns and arches.

Let us consider the kth element of an arch, shown in Fig. 3.1. The element is mapped from the standard quadrilateral element, also shown in Fig. 3.1, by some smooth mapping functions:

$$x = x^{(k)}(\xi, \eta), \qquad y = y^{(k)}(\xi, \eta), \qquad (\xi, \eta) \in \Omega_{st} \tag{3.1a}$$

where Ω_{st} is the standard element and the superscript (k) refers to the kth finite element, Ω_k. The inverse mapping is:

$$\xi = \xi^{(k)}(x, y), \qquad \eta = \eta^{(k)}(x, y), \qquad (x, y) \in \Omega_k. \tag{3.1b}$$

In the following we omit the superscript (k) with the understanding that the discussion refers to the kth element.

In the case of beam-columns and arches one dimension is generally much larger than the other two. We will assume that the lines corresponding to constant η values $(-1 < \xi < 1)$ are in the "long" direction of the curved beam or arch.

Let us now consider an arbitrary point P, as shown in Fig. 3.1. Point P is located at the intersection of two coordinate lines, one corresponding to constant ξ, the other corresponding to constant η values. We denote the unit vector which is tangent to the constant η line by $\vec{e}_\xi$ and the unit vector which is tangent to the constant ξ line by $\vec{e}_\eta$. Given the mapping (3.1) the normalized covariant basis vectors are:

$$\vec{e}_\xi = \frac{1}{\sqrt{\left(\frac{\partial x}{\partial \xi}\right)^2 + \left(\frac{\partial y}{\partial \xi}\right)^2}} \left\{ \frac{\partial x}{\partial \xi} \quad \frac{\partial y}{\partial \xi} \right\}^T \tag{3.2a}$$

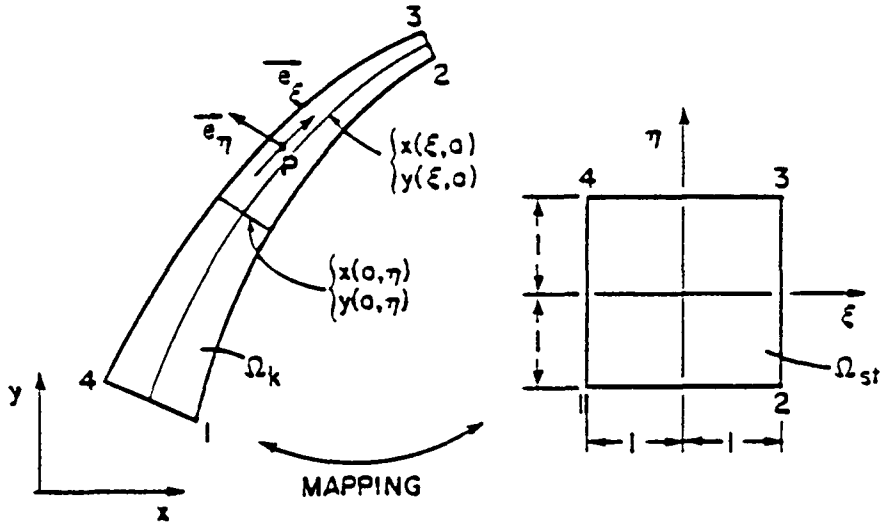

Fig. 3.1. Typical arch element. Notation.

$$\vec{e}_\eta = \frac{1}{\sqrt{\left(\frac{\partial x}{\partial \eta}\right)^2 + \left(\frac{\partial y}{\partial \eta}\right)^2}} \left\{ \frac{\partial x}{\partial \eta} \quad \frac{\partial y}{\partial \eta} \right\}^T . \tag{3.2b}$$

Note that $\vec{e}_\xi$ is generally not orthogonal to $\vec{e}_\eta$.

We denote the displacement vector components in the direction of $\vec{e}_\xi$ (resp. $\vec{e}_\eta$) by u_ξ (resp. u_η). Similarly, we denote the displacement vector components in the direction of x (resp. y) by u_x (resp. u_y). The components u_x, u_y are related to u_ξ, u_η by the following relationships:

$$u_x = \frac{1}{\sqrt{\left(\frac{\partial x}{\partial \xi}\right)^2 + \left(\frac{\partial y}{\partial \xi}\right)^2}} \frac{\partial x}{\partial \xi} u_\xi + \frac{1}{\sqrt{\left(\frac{\partial x}{\partial \eta}\right)^2 + \left(\frac{\partial y}{\partial \eta}\right)^2}} \frac{\partial x}{\partial \eta} u_\eta \tag{3.3a}$$

$$u_y = \frac{1}{\sqrt{\left(\frac{\partial x}{\partial \xi}\right)^2 + \left(\frac{\partial y}{\partial \xi}\right)^2}} \frac{\partial y}{\partial \xi} u_\xi + \frac{1}{\sqrt{\left(\frac{\partial x}{\partial \eta}\right)^2 + \left(\frac{\partial y}{\partial \eta}\right)^2}} \frac{\partial y}{\partial \eta} u_\eta . \tag{3.3b}$$

We now introduce the notation:

$$\{u\}_{(x,y)} \stackrel{\text{def}}{=} \begin{Bmatrix} u_x \\ u_y \end{Bmatrix}, \qquad \{u\}_{(\xi,\eta)} \stackrel{\text{def}}{=} \begin{Bmatrix} u_\xi \\ u_\eta \end{Bmatrix}. \tag{3.4}$$

With this notation (3.3a,b) can be written as:

$$\{u\}_{(x,y)} = [R]\{u\}_{(\xi,\eta)} \tag{3.5}$$

where the definition of the 2×2 matrix $[R]$ is obvious from (3.3a,b).

We now define space $S^{p,q}$ to be the *span* of the following $(p+1)(q+1)$ monomials on the standard quadrilateral element:

$$1,\ \xi,\ \xi^2,\ \ldots,\ \xi^p,$$

$$\eta,\ \xi\eta,\ \xi^2\eta,\ \ldots,\ \xi^p\eta,$$

$$\vdots$$

$$\eta^q,\ \xi\eta^q,\ \xi^2\eta^q,\ \ldots,\ \xi^p\eta^q.$$

For example, the spanning set for $S^{4,2}$ is the set of monomials inside the dotted lines in Fig. 3.2.

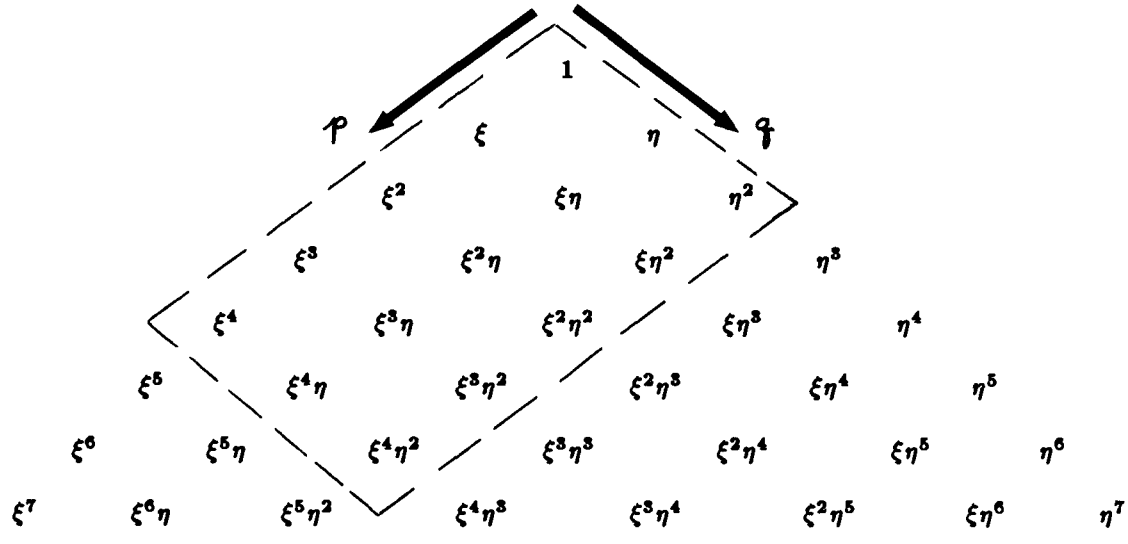

Fig. 3.2. Space $S^{4,2}$ is spanned by the monomial terms inside the dotted lines.

We denote the dimension of $S^{p,q}$ by n, that is:

$$n \stackrel{\text{def}}{=} \dim S^{p,q} = (p+1)(q+1). \tag{3.6}$$

We define n basis functions for $S^{p,q}$ and denote these basis functions by $N_i(\xi,\eta)$, $i = 1, 2, \ldots, n$. The definition of basis functions is given in Section 4. Thus any

function u, defined on the standard element Ω_{st}, which lies in $S^{p,q}$ can be written in the form:

$$u = \sum_{i=1}^{n} a_i N_i(\xi, \eta) \tag{3.7}$$

where a_i are arbitrary real numbers. We remark that in the finite element method a_i are not completely arbitrary because interelement continuity constraints and constraints that represent kinematic (principal) boundary conditions must be enforced. Although the basis functions are defined on the standard domain, and are given in terms of the standard variables ξ and η, we can (at least in principle) substitute (3.1b) for ξ and η and view the basis functions as functions defined on Ω_k.

We will investigate two approaches: In the first approach the approximations to the curvilinear components of the displacement vector u_ξ, u_η lie in $S^{p,q}$. In the second approach the approximations to the Cartesian components of the displacement vector u_x, u_y lie in $S^{p,q}$. The first is the classical approach. Its main advantage is that for certain types of mapping analytical solutions can be obtained. Also, in this approach different degrees of approximation can be used for the displacement components. For example, in the Reissner-Mindlin theory $u_\xi \in S^{p,1}$ and $u_\eta \in S^{p,0}$. Note that index q identifies a particular beam or arch theory within the hierarchic system of theories whereas index p identifies a particular discretization within a hierarchic sequence of discretizations based on p-extension. The second approach is better suited for computer implementation because enforcement of the appropriate continuity conditions between elements mapped by different mapping functions, a condition which frequently occurs in engineering applications, is simpler. This permits the use of a great variety of mapping functions. Also, computation of the stiffness matrices and load vectors as well as post-solution procedures are somewhat simpler. On the other hand, when Cartesian systems are used then the displacement components are not oriented in the long and short dimensions in general. Therefore the same degree of approximation has to be used for each displacement component. While this increases the computational work somewhat, an important advantage is gained: all monomial terms which contain η, η^2, ..., η^q are retained in the approximation.

When we approximate the curvilinear components we have:

$$\begin{Bmatrix} u_\xi \\ u_\eta \end{Bmatrix} = \begin{bmatrix} N_1 & N_2 & \dots & N_n & 0 & 0 & \dots & 0 \\ 0 & 0 & \dots & 0 & N_1 & N_2 & \dots & N_m \end{bmatrix} \begin{Bmatrix} a_1 \\ a_2 \\ \vdots \\ a_{n+m} \end{Bmatrix} \tag{3.8a}$$

or, in short hand:

$$\{u\}_{(\xi,\eta)} = [N]\{a\} \tag{3.8b}$$

where a_1, a_2 ..., a_{n+m} are coefficients to be determined from the finite element solution. When we refer to a specific element, for example the kth element, we write: $a_i^{(k)}$ $(i = 1, 2, \dots, n+m)$ or, simply, $\{a^{(k)}\}$. We denote individual columns of $[N]$ by $\{N_i\}$. Thus we can also write (3.8a,b) in the following form:

$$\{u\}_{(\xi,\eta)} = \sum_{i=1}^{n+m} a_i \{N_i\}. \tag{3.8c}$$

When we approximate the Cartesian components then the expressions are similar but we must have $n = m$:

$$\{u\}_{(x,y)} = \sum_{i=1}^{2n} a_i \{N_i\}. \tag{3.9}$$

We remark that if we accept the restriction $n = m$ then the two approaches can be interpreted as the choice of the space $S^{p,q}$: When the curvilinear components are approximated then $\{u\}_{(x,y)} \in S^{p,q}$ where $S^{p,q}$ is spanned by $[R]\{N_i\}$, $i = 1, 2, \dots 2n$. When the Cartesian components are approximated then $\{u\}_{(x,y)} \in S^{p,q}$ where $S^{p,q}$ is spanned by $\{N_i\}$, $i = 1, 2, \dots 2n$. We now describe the computation of elemental stiffness matrices and load vectors for both cases.

3.1.1. Element stiffness matrices.

The strain energy of the kth element is of the form:

$$U_k \stackrel{\text{def}}{=} \frac{1}{2} \iint_{\Omega_k} (\sigma_x \epsilon_x + \sigma_y \epsilon_y + \tau_{xy} \gamma_{xy})\, t\, dx\, dy = \frac{1}{2} \iint_{\Omega_k} \left([D]\{u\}_{(x,y)}\right)^T [E][D]\{u\}_{(x,y)}\, t\, dx\, dy \tag{3.10}$$

where σ_x, σ_y, τ_{xy} are the stress components, ϵ_x, ϵ_y, γ_{xy} are the strain components, $t = t(x, y)$ is the thickness; $[D]$ is a differential operator matrix. In the case of plane

elasticity:

$$[D] = \begin{bmatrix} \frac{\partial}{\partial x} & 0 \\ 0 & \frac{\partial}{\partial y} \\ \frac{\partial}{\partial y} & \frac{\partial}{\partial x} \end{bmatrix}. \tag{3.11}$$

[E] is the *material stiffness matrix*. For example, in the case of *plane stress:*

$$[E] = \frac{E}{(1-\nu^2)} \begin{bmatrix} 1 & \nu & 0 \\ \nu & 1 & 0 \\ 0 & 0 & \frac{1-\nu}{2} \end{bmatrix} \tag{3.12}$$

where E and ν are, respectively, the modulus of elasticity and Poisson's ratio.

We now transform the integral (3.10) so that the integration is on the standard element Ω_{st}. We denote the Jacobian matrix of the transformation (3.1a) by $[J]$ and its inverse by $[J^*]$:

$$[J] \stackrel{\text{def}}{=} \begin{bmatrix} J_{11} & J_{12} \\ J_{21} & J_{22} \end{bmatrix} \stackrel{\text{def}}{=} \begin{bmatrix} \frac{\partial x}{\partial \xi} & \frac{\partial y}{\partial \xi} \\ \frac{\partial x}{\partial \eta} & \frac{\partial y}{\partial \eta} \end{bmatrix}, \qquad [J]^{-1} \stackrel{\text{def}}{=} [J^*] \stackrel{\text{def}}{=} \begin{bmatrix} J^*_{11} & J^*_{12} \\ J^*_{21} & J^*_{22} \end{bmatrix} \tag{3.13}$$

and we denote the determinant of the Jacobian matrix by $|J|$. We define:

$$[D^*] \stackrel{\text{def}}{=} \begin{bmatrix} J^*_{11}\frac{\partial}{\partial \xi} + J^*_{12}\frac{\partial}{\partial \eta} & 0 \\ 0 & J^*_{21}\frac{\partial}{\partial \xi} + J^*_{22}\frac{\partial}{\partial \eta} \\ J^*_{21}\frac{\partial}{\partial \xi} + J^*_{22}\frac{\partial}{\partial \eta} & J^*_{11}\frac{\partial}{\partial \xi} + J^*_{12}\frac{\partial}{\partial \eta} \end{bmatrix}. \tag{3.14}$$

Clearly, $[D^*]$ is $[D]$ written in terms of the variables ξ and η. When we approximate the Cartesian components of the displacement vector then we can write (3.10) in the following form:

$$U_k = \frac{1}{2} \iint_{\Omega_{st}} \left([D^*]\{u\}_{(x,y)}\right)^T [E][D^*]\{u\}_{(x,y)}\, t\, |J|\, d\xi\, d\eta. \tag{3.15a}$$

The subscript k is a reminder that $[D^*]$ and $|J|$ are computed from the mapping functions of the kth element. When we approximate the curvilinear components of the displacement vector then from (3.5) and (3.15a) we have:

$$U_k = \frac{1}{2} \iint_{\Omega_{et}} \left([D^*][R]\{u\}_{(\xi,\eta)}\right)^T [E][D^*][R]\{u\}_{(\xi,\eta)}\, t\, |J|\, d\xi\, d\eta. \tag{3.15b}$$

The stiffness matrix for the kth element is defined so that:

$$U_k = \frac{1}{2}\{a^{(k)}\}^T [K^{(k)}]\{a^{(k)}\} \tag{3.16}$$

therefore, when we approximate the Cartesian displacement components then the elements of $[K^{(k)}]$ are:

$$k_{ij}^{(k)} = \iint_{\Omega_{et}} ([D^*]\{N_i\})^T [E][D^*]\{N_j\}\, t\, |J|\, d\xi\, d\eta. \tag{3.17a}$$

When we approximate the curvilinear displacement components then the elements of $[K^{(k)}]$ are:

$$k_{ij}^{(k)} = \iint_{\Omega_{et}} ([D^*][R]\{N_i\})^T [E][D^*][R]\{N_j\}\, t\, |J|\, d\xi\, d\eta. \tag{3.17b}$$

These terms are usually computed by numerical quadrature. However when the mapping is linear then the integrations can be performed in closed form and the speed of computation greatly increased. See, for example, [19,20].

3.1.2. Element load vectors: traction loading.

Let us assume that the load is known in terms of traction components applied in the normal and tangential directions on the upper surface of the beam-column or arch, that is on the surface corresponding to $\eta = 1$, see Fig. 3.1 and (3.1a). We will consider this case only, the other cases are treated analogously. By definition, the potential of external traction loads acting on element Ω_k is:

$$P_k = \int_{\partial\Omega_k} (T_x\, u_x + T_y\, u_y)\, dS \tag{3.18}$$

where $\partial\Omega_k$ represents the bounding surfaces of element k; T_x, T_y are components of the traction vector; dS is the differential surface. We will write dS in terms of the differential arclength ds and the thickness: $dS = t\, ds$ (see Fig. 3.3). In practical problems usually T_n and T_t rather than T_x and T_y are given. Referring to Fig. 3.3 we have:

$$\begin{Bmatrix} T_x \\ T_y \end{Bmatrix} = \begin{bmatrix} \cos\alpha & -\sin\alpha \\ \sin\alpha & \cos\alpha \end{bmatrix} \begin{Bmatrix} T_n \\ T_t \end{Bmatrix}. \tag{3.19}$$

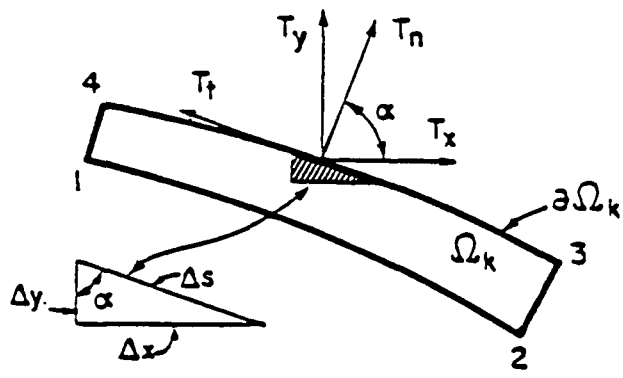

Fig. 3.3. Notation: Traction vector components.

From the definition of α in Fig. 3.4 we have:

$$\sin\alpha = -\frac{dx}{ds}; \qquad \cos\alpha = \frac{dy}{ds} \tag{3.20}$$

and, from (3.1a):

$$dx = \frac{\partial x^{(k)}}{\partial \xi}\Big|_{\eta=1} d\xi; \qquad dy = \frac{\partial y^{(k)}}{\partial \xi}\Big|_{\eta=1} d\xi. \tag{3.21}$$

Therefore we can write:

$$P_k = \int_{-1}^{+1} \{u\}^T_{(x,y)} \begin{bmatrix} \dfrac{\partial y^{(k)}}{\partial \xi} & \dfrac{\partial x^{(k)}}{\partial \xi} \\ -\dfrac{\partial x^{(k)}}{\partial \xi} & \dfrac{\partial y^{(k)}}{\partial \xi} \end{bmatrix}_{\eta=1} \begin{Bmatrix} T_n \\ T_t \end{Bmatrix} t\, d\xi. \tag{3.22}$$

If we work in a Cartesian system we substitute:

$$\{u\}_{x,y} = [N]\{a\} \tag{3.23a}$$

or, if we work in the curvilinear system, we substitute:

$$\{u\}_{x,y} = [R][N]\{a\} \tag{3.23b}$$

into (3.22) and write P_k in the following form:

$$P_k = \{a\}^T \{r^{(k)}\} \tag{3.24a}$$

where $\{r^{(k)}\}$ is the *load vector* of the kth element. Thus, when the Cartesian components of the displacement vector are approximated, the ith element of the load vector of the kth finite element is:

$$r_i^{(k)} = \int_{-1}^{+1} \{N_i\}^T \begin{bmatrix} \frac{\partial y^{(k)}}{\partial \xi} & \frac{\partial x^{(k)}}{\partial \xi} \\ -\frac{\partial x^{(k)}}{\partial \xi} & \frac{\partial y^{(k)}}{\partial \xi} \end{bmatrix}_{\eta=1} \begin{Bmatrix} T_n \\ T_t \end{Bmatrix} t \, d\xi. \tag{3.24b}$$

3.2. Plates and shells.

The computation of stiffness matrices and load vectors for plate and shell elements is analogous to the procedure described in Section 3.1. Plate and shell elements are usually six sided but five sided elements are often useful also. We will consider six-sided elements only, thus the standard element is the hexahedron, shown in Fig. 3.3. The mapping functions are:

$$x = x^{(k)}(\xi, \eta, \varsigma), \quad y = y^{(k)}(\xi, \eta, \varsigma), \quad z = z^{(k)}(\xi, \eta, \varsigma), \quad -1 < \xi, \eta, \varsigma < 1. \tag{3.25}$$

We will assume the mapping to be so that $\varsigma = 0$ is the middle surface of the shell. Thus $\varsigma = +1$ gives the 'upper' surface and $\varsigma = -1$ the 'lower' surface of the shell. In the following we will omit the superscript (k).

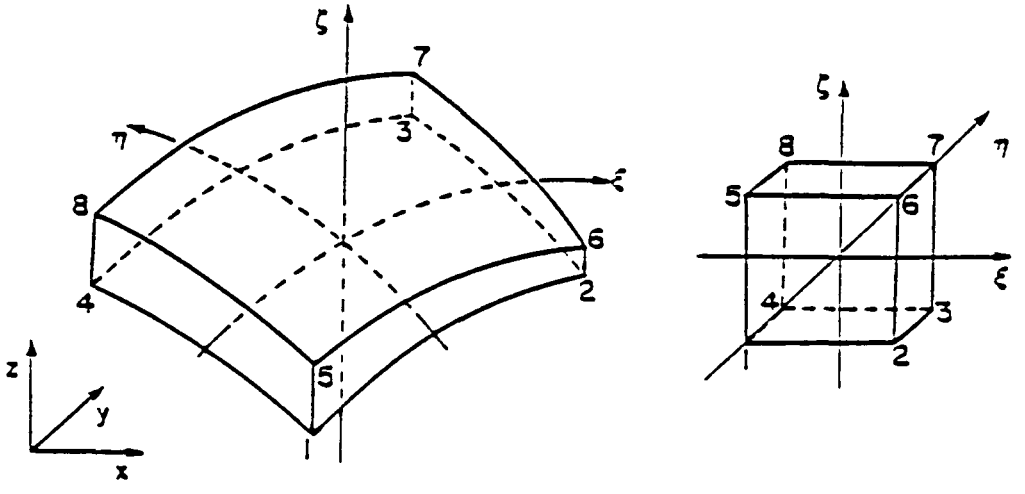

Fig. 3.4. Typical shell element. Notation.

The strain energy of the kth element is:

$$U_k \stackrel{\text{def}}{=} \frac{1}{2}\iiint_{\Omega_k} (\sigma_x\epsilon_x + \sigma_y\epsilon_y + \sigma_z\epsilon_z + \tau_{xy}\gamma_{xy} + \tau_{yz}\gamma_{yz} + \tau_{zx}\gamma_{zx})\,dx\,dy\,dz$$
$$= \frac{1}{2}\iiint_{\Omega_k} \left([D]\{u\}_{(x,y,z)}\right)^T [E][D]\{u\}_{(x,y,z)}\,dx\,dy\,dz \tag{3.26}$$

where $\{u\}_{(x,y,z)} \stackrel{\text{def}}{=} \{u_x\ u_y\ u_z\}^T$ is the displacement vector; $[D]$ is the differential operator matrix of the three dimensional strain-displacement relationship and [E] is the stress-strain law in three dimensions. The definitions are analogous to those in (3.11), (3.12) and the details are available in every textbook on elasticity and strength of materials.

Once again we have the option of approximating either the curvilinear or Cartesian components of the displacement vector. The relationship between the curvilinear and Cartesian components is analogous to (3.5). Thus the approximation is either:

$$\{u\}_{(\xi,\eta,\zeta)} = [N]\{a\} \tag{3.27a}$$

where $[N]$ is a $3 \times (2n + m)$ matrix of basis functions; or:

$$\{u\}_{(x,y,z)} = [N]\{a\} \tag{3.27b}$$

where $[N]$ is a $3 \times 3n$ matrix of basis functions. The basis functions are defined on the standard hexahedral element. The space spanned by the basis functions is denoted by $\mathcal{S}^{p,p,q}$. Basis functions, based on Legendre polynomials, are defined in the following section. Equation (3.27a) represents the conventional approach.

3.3. Laminated arches and shells.

In this paper we are primarily concerned with homogeneous arches and shells. In the case of laminated arches and shells the normal and shear stresses are continuous across laminar interfaces but the strains are not. Three approaches are possible:

(1) The arch or shell elements can be "stacked" so that the laminar interfaces correspond to interelement boundaries. This is feasible when there are only a few laminae, as in the case of arches and shells of sandwich construction.

(2) When there are many laminae and interlaminar stresses are of interest then the mapping should be so that the laminar interfaces correspond to constant η lines in two dimensions or constant ς surfaces in three dimensions. In this case $N_i(\xi, \eta)$ in two dimensions (resp. $N_i(\xi, \eta, \varsigma)$ in three dimensions) must be piecewise polynomials in the η (resp. ς) direction which are continuous at the laminar interfaces, with discontinuous derivatives. The derivative ratios are computed so that the condition of continuity of the normal and shear stresses is satisfied.

(3) When there are many laminae and the interlaminar stresses are not of interest then the material can be treated as homogeneous, and the material properties chosen to represent average properties of the laminae.

4. HIERARCHIC BASIS FUNCTIONS FOR $S^{p,q}$ AND $S^{p,p,q}$.

The key considerations in the selection of basis functions are to ensure numerical stability and to make the computational effort required for the generation of stiffness matrices and load vectors as small as possible. We wish to perform p-extensions, therefore the basis functions should be *hierarchic*, that is the basis functions corresponding to polynomial degree p ($p > 1$) should contain, as subsets, the basis functions corresponding to polynomal degrees $p-1$, $p-2$, ..., 1. Computational experience has shown that basis functions based on Legendre polynomials have good properties from the point of view of numerical stability. We also wish to construct our basis functions in such a way that curved beam elements can be readily joined with plane elastic elements and plate and shell elements can be readily joined with three dimensional finite elements. In the following we define the basis functions used for $S^{p,q}$ and $S^{p,p,q}$ in the present investigation.

4.1. Hierarchic basis functions for $S^{p,q}$.

The basis functions for $S^{1,1}$ are the usual basis functions for four-noded quadrilateral finite elements:

$$\begin{aligned} \overset{\circ}{N}_1 &= \frac{1}{4}(1-\xi)(1-\eta) \qquad & \overset{\circ}{N}_3 &= \frac{1}{4}(1+\xi)(1+\eta) \\ \overset{\circ}{N}_2 &= \frac{1}{4}(1+\xi)(1-\eta) \qquad & \overset{\circ}{N}_4 &= \frac{1}{4}(1-\xi)(1+\eta) \end{aligned} \tag{4.1}$$

where the superscript ($\circ$) indicates that these basis functions are associated with the vertices which are domains of dimension zero. We now define:

$$\phi_i(\xi) = \sqrt{\frac{2i-1}{2}} \int_{-1}^{\xi} P_{i-1}(t)\, dt \qquad i = 2, 3, \ldots, p \tag{4.2}$$

where P_1, P_2, ..., P_{p-1} are the *Legendre polynomials*. The basis functions for $S^{p,1}$, $p > 1$ are comprised of the four vertex modes (4.1) and the following functions associated with the sides corresponding to $\eta = \pm 1$, hence are usually referred to as *side modes*:

$$\overset{1}{N}_{2i-3} = \frac{1-\eta}{2}\phi_i(\xi), \qquad \overset{1}{N}_{2i-2} = \frac{1+\eta}{2}\phi_i(\xi), \qquad i = 2, 3, \ldots, p \tag{4.3}$$

The basis functions for $S^{p,q}$, $q > 1$ are comprised of the basis functions for $S^{p,1}$ plus the following edge modes:

$$\overset{1}{N}_{2p+2j-3} = \frac{1-\xi}{2}\phi_j(\eta), \qquad \overset{1}{N}_{2p+2j-2} = \frac{1+\xi}{2}\phi_j(\eta), \qquad j = 2, 3, \ldots, q \tag{4.4}$$

and, when $p, q \geq 2$, we have the following basis functions, called *internal modes*:

$$\overset{2}{N}_k = (1-\xi^2)(1-\eta^2)P_i(\xi)P_j(\eta), \qquad i = 0, 1, 2, \ldots, p-2; \quad j = 0, 1, 2, \ldots, q-2 \tag{4.5}$$

where the superscript 2 indicates that these basis functions are associated with the area of the standard quadrilateral element which is a domain of dimension two. The subscript k ranges from 1 to $(p-1)(q-1)$.

In summary, we have four nodal basis functions, given by (4.1); $2(p-1)+2(q-1)$ edge modes, given by (4.3) and (4.4); $(p-1)(q-1)$ internal modes $(p, q \geq 2)$, given by (4.5), a total of $(p+1)(q+1)$ basis functions, which is the dimension of $S^{p,q}$. These basis functions are polynomials and are linearly independent. There are no monomial terms in the basis functions which are not in the spanning set for $S^{p,q}$. Therefore these basis functions also span $S^{p,q}$.

4.2. Hierarchic basis functions for $S^{p,p,q}$.

4.2.1. The vertex modes: Basis functions for $S^{1,1,1}$.

There are 8 vertex modes, denoted by $\overset{\circ}{N}_i$, $i = 1, 2, \ldots, 8$. Once again the superscript $(^\circ)$ indicates that these modes are associated with the vertices which are of dimension zero:

$$\overset{\circ}{N}_1 = \frac{1}{8}(1-\xi)(1-\eta)(1-\varsigma) \tag{4.6a}$$

$$\overset{\circ}{N}_2 = \frac{1}{8}(1+\xi)(1-\eta)(1-\varsigma) \tag{4.6b}$$

$$\vdots$$

$$\overset{\circ}{N}_8 = \frac{1}{8}(1-\xi)(1-\eta)(1+\varsigma). \tag{4.6c}$$

4.2.2. Edge modes.

We use the superscript 1 to indicate that the edge modes pertain to the edges which are of dimension one.

(a) In the case of $S^{p,p,1}$ $(p \geq 2)$ there are $8(p-1)$ edge modes. These are defined in terms of the function ϕ_i, see (4.2):

$$\overset{1}{N}_{1+8(i-2)} = \frac{1}{4}\phi_i(\xi)(1-\eta)(1-\varsigma) \tag{4.7a}$$

$$\overset{1}{N}_{2+8(i-2)} = \frac{1}{4}\phi_i(\eta)(1+\xi)(1-\varsigma) \tag{4.7b}$$

$$\vdots$$

$$\overset{1}{N}_{8+8(i-2)} = \frac{1}{4}\phi_i(\eta)(1-\xi)(1+\varsigma) \tag{4.7c}$$

where $i = 2, 3, \ldots, p$.

(b) In the case of $S^{p,p,q}$ $(p \geq 2,\ q \geq 2)$ there are $8(p-1)+4(q-1)$ edge modes. These are defined as follows:

$$\overset{1}{N}_{1+8(i-2)} = \frac{1}{4}\phi_i(\xi)(1-\eta)(1-\varsigma) \tag{4.8a}$$

$$\overset{1}{N}_{2+8(i-2)} = \frac{1}{4}\phi_i(\eta)(1+\xi)(1-\varsigma) \tag{4.8b}$$

$$\vdots$$

$$\overset{1}{N}_{8+8(i-2)} = \frac{1}{4}\phi_i(\eta)(1-\xi)(1+\varsigma) \tag{4.8c}$$

$$\overset{1}{N}_{9+4(j-2)} = \frac{1}{4}\phi_j(\varsigma)(1-\xi)(1-\eta) \tag{4.8d}$$

$$\overset{1}{N}_{10+4(j-2)} = \frac{1}{4}\phi_j(\varsigma)(1+\xi)(1-\eta) \tag{4.8e}$$

$$\overset{1}{N}_{11+4(j-2)} = \frac{1}{4}\phi_j(\varsigma)(1+\xi)(1+\eta) \tag{4.8f}$$

$$\overset{1}{N}_{12+4(j-2)} = \frac{1}{4}\phi_j(\varsigma)(1-\xi)(1+\eta) \tag{4.8g}$$

where $i = 2, 3, \ldots, p$; $j = 2, 3, \ldots, q$.

4.2.3. Face modes.

We use the superscript 2 to indicate that the face modes pertain to faces which are of dimension two. The hierarchic face modes can be treated in one of two ways: Either all face modes are analogous to the internal modes (4.5), in which case there are $2(p-1)^2 + 4(p-1)(q-1)$ face modes, $p, q \geq 2$, or only the face

modes which are nonvanishing on faces $\xi = \pm 1$; $\eta = \pm 1$ are analogous to (4.5) and the face modes which are nonvanishing on faces $\varsigma = \pm 1$ are defined by:

$$\overset{2}{N}_m = \frac{1}{2}(1-\xi^2)(1-\eta^2)(1\pm\varsigma)P_i(\xi)P_j(\eta) \quad i,j = 0,1,\ldots,p-4; \quad (i+j) = 0,1,\ldots,p-4 \tag{4.9}$$

and $m = m(i,j)$ depends on the numbering scheme used. In this case the number of face modes (n_f) is:

$$n_f = \begin{cases} 4(p-1)(q-1) & \text{for } p = 2,3 \\ 4(p-1)(q-1) + (p-2)(p-3) & \text{for } p \geq 4. \end{cases} \tag{4.10}$$

This is analogous to the definition of hierarchic internal modes in the case of plane elastic elements [21,22].

4.2.4. Internal modes.

We identify the internal modes by the superscript 3. There are $(p-3)(p-2)(q-1)/2$ internal modes $(p \geq 4;\ q \geq 2)$, defined as follows:

$$\overset{3}{N}_m = (1-\xi^2)(1-\eta^2)(1-\varsigma^2)P_i(\xi)P_j(\eta)P_k(\varsigma) \tag{4.11a}$$

where:

$$i,j = 0,1,\ldots,p-4; \quad (i+j) = 0,1,\ldots,p-4; \quad k = 0,1,\ldots,q-2 \tag{4.11b}$$

and $m = m(i,j,k)$ depends on the numbering scheme used.

5. EXAMPLES.

The following examples illustrate p-extension procedures and demonstrate that conventional curvilinear bases can be replaced by Cartesian bases for a wide range of radius to thickness ratios without significant loss in performance. Extension procedures are the only means available for the estimation and control of errors of discretization. Here we are interested in ensuring that the stress resultants (i.e. membrane forces, shear forces and moments) are accurate to within one percent relative error.

We report the percent estimated relative error in energy norm, denoted by $(e_r)_E$. These estimates are based on the theoretical estimate of error for p-extensions. The constants in the theoretical estimate can be computed once the strain energies have been computed from finite element solutions corresponding to three polynomial degrees $p-2,\ p-1,\ p;\ p \geq 3$. Details are available in [21,23,24]. The estimated exact values of the strain energy were computed by the computer program *PROBE* [21].

In all example problems the mapping functions were generated by the *blending function method* [21]. Thus circular arcs and cylindrical surfaces were represented exactly.

5.1. Circular arch, constant cross section, r/t≈15.

Our first example is the moderately thick circular arch shown in Fig. 5.1. The thickness of the arch, i.e. its dimension perpendicular to the x,y plane, is unity. It is loaded by parabolically distributed shearing traction in the plane of symmetry so that the shear stresses vanish at the top and bottom surfaces and $F_{BY} = -1.0$. Poisson's ratio is zero. The goal of computation is to determine the stress resultants F_{AX}, F_{AY}, M_{A0}, F_{BX} and M_{B0}. By definition:

$$F_X = \int_A (\sigma_x \cos\alpha + \tau_{xy} \sin\alpha)\, dA \tag{5.1a}$$

where A is the cross sectional area and α is the angle measured from the positive x axis to the outward normal to the cross section. Similarly:

$$F_Y = \int_A (\tau_{xy} \cos\alpha + \sigma_y \sin\alpha)\, dA \tag{5.1b}$$

and

$$M_0 = \int_A [(\tau_{xy} \cos\alpha + \sigma_y \sin\alpha)\, x - (\sigma_x \cos\alpha + \tau_{xy} \sin\alpha)\, y]\, dA. \tag{5.1c}$$

The stress resultants were computed from the finite element solutions directly by numerical quadrature using twelve Gaussian quadrature points on each boundary segment. Of course, the computed stress resultants are not independent. From the equations of statics we have:

$$F_{AX} = -F_{BX}, \quad F_{AY} = -F_{BY} = 1.000, \quad M_{A0} = -M_{B0}. \tag{5.2}$$

The exact solution is not known. To obtain a good approximation to the exact solution, we solved this as a problem in two dimensional elasticity. The computer program *PROBE* was used [21]. In *PROBE* the standard polynomial space for quadrilateral elements is spanned by all monomial terms of degree p plus the terms $\xi^p\eta$ and $\xi\eta^p$ for $p \geq 2$. The maximal value of p is 8. Details, including the definition of element level basis functions, are available in [21,22]. The results for $p = 1, 2, \ldots, 8$ are shown in Table 5.1. We see that at $p = 8$ the equations of equilibrium are satisfied to at least four digits. The estimated exact value of the strain energy, determined from a sequence of fully two dimensional finite element solutions by *PROBE*, is $0.146660 \times 10^3/E$ where E is the modulus of elasticity.

Table 5.1. Circular arch, constant cross section, 3 elements. $r/t \approx 15$.
Solution as a problem of elasticity.

p	N	$(e_r)_E$	F_{AX}	F_{AY}	M_A	F_{BX}	F_{BY}	M_B
3	44	14.9	2.760	1.950	−46.17	3.366	−1.547	51.58
4	67	6.1	1.653	1.141	−28.17	−1.732	−0.984	28.07
5	96	3.6	1.577	0.996	−25.82	−1.577	−0.996	25.81
6	131	2.5	1.580	1.000	−25.86	−1.580	−0.999	25.86
7	172	1.9	1.580	1.000	−25.86	−1.580	−0.999	25.86
8	219	1.5	1.580	1.000	−25.86	−1.580	−1.000	25.86

In this problem the estimated error in energy norm is related to the error in the average displacement of the loaded cross section. Because by definition the energy norm of the error is the *square root* of the strain energy of the error, 10 percent error in energy norm corresponds to 1 percent error in the displacement. For $q = 1$ and $q = 2$ the error in energy norm is virtually constant as p is increased.

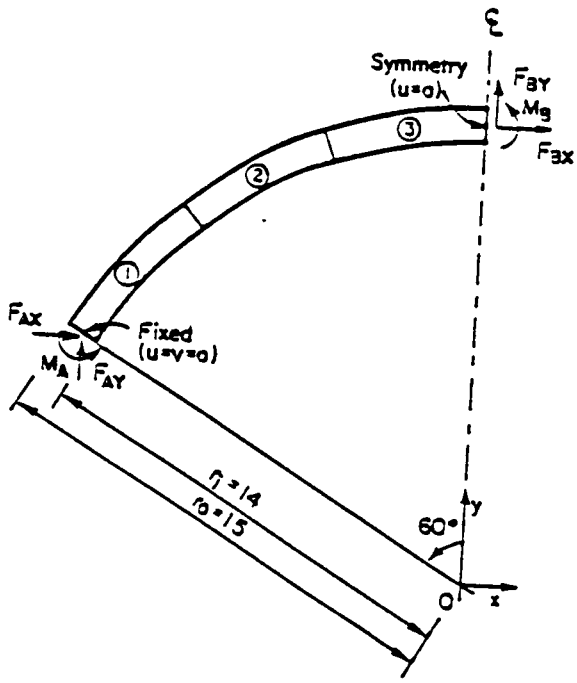

Fig. 5.1. Circular arch.

For $q = 3$ there is a substantial decrease of error. This is due to the fact that at $q = 3$ representation of the shear deformation is greatly improved. In general, if the estimated relative error in energy norm is not changing as p is increased while q is held constant, then virtually all of the error in energy norm is caused by the fact that q is too low. However, as the results in Table 5.2 indicate, large error in energy norm does not necessarily mean that the error in stress resultants or other quantities of interest is large. The converse of this statement is also true, see for example [24]. At $(p, q) = (5, 1)$ the estimated relative error in energy norm is 7.9 percent, that is 0.079. The relative error of the displacement of the loaded cross section is is $0.079^2 = 0.0062$, that is 0.62 percent. This level of precision is usually more than adequate in elastostatics. In elastodynamics on the other hand, computation of the high frequency displacement modes necessitates greater precision and thus higher q values.

5.2. Circular arch, constant cross section, r/t≈1000.

Our second example is similar to the first, except the arch is now thin: We have changed the r_i from 14.0 to 14.985, see Fig. 5.1. We examine two cases: In

Table 5.2 Circular arch, constant thickness, 3 elements. $r/t \approx 15$.
(a) Curvilinear basis.

p,q	N	$(e_r)_E$	F_{AX}	F_{AY}	M_{A0}	F_{BX}	F_{BY}	M_{B0}
3,1	34	11.2	1.668	0.370	−18.45	−0.942	−1.370	16.48
4,1	46	7.9	1.555	0.969	−25.30	−1.544	−0.991	25.33
5,1	58	7.9	1.580	1.001	−25.88	−1.582	−0.999	25.88
6,1	70	7.9	1.581	1.000	−25.87	−1.581	−1.000	25.87
7,1	82	7.9	1.581	1.000	−25.87	−1.581	−1.000	25.87
8,1	94	7.9	1.581	1.000	−25.87	−1.581	−1.000	25.87
3,2	51	11.2	1.668	0.370	−18.45	−0.942	−1.370	16.48
4,2	69	7.9	1.555	0.969	−25.30	−1.544	−0.991	25.33
5,2	87	7.9	1.581	1.001	−25.88	−1.582	−0.999	25.88
6,2	105	7.9	1.581	1.000	−25.87	−1.581	−1.000	25.87
7,2	123	7.9	1.581	1.000	−25.87	−1.581	−1.000	25.87
8,2	141	7.8	1.581	1.000	−25.87	−1.581	−1.000	25.87
3,3	68	8.5	1.684	0.356	−18.39	−0.937	−1.396	16.40
4,3	92	2.0	1.580	0.952	−25.25	−1.541	−1.025	25.28
5,3	116	1.6	1.603	0.986	−25.84	−1.579	−1.029	25.84
6,3	140	1.3	1.600	0.988	−25.84	−1.579	−1.023	25.84
7,3	164	1.1	1.596	0.990	−25.85	−1.580	−1.016	25.85
8,3	188	1.0	1.591	0.993	−25.85	−1.580	−1.009	25.85

(b) Cartesian basis.

p,q	N	$(e_r)_E$	F_{AX}	F_{AY}	M_{A0}	F_{BX}	F_{BY}	M_{B0}
3,1	34	15.8	2.761	1.950	−46.18	−3.367	−1.547	51.58
4,1	46	8.0	1.653	1.141	−28.18	−1.733	−0.984	28.08
5,1	58	7.9	1.576	1.000	−25.83	−1.577	−0.996	25.82
6,1	70	7.9	1.580	1.000	−25.87	−1.581	−1.000	25.87
7,1	82	7.9	1.581	1.000	−25.87	−1.581	−1.000	25.87
8,1	94	7.9	1.581	1.000	−25.87	−1.581	−1.000	25.87
3,2	51	15.8	2.761	1.950	−46.18	−3.367	−1.547	51.58
4,2	69	8.0	1.653	1.142	−28.18	−1.733	−0.984	28.08
5,2	87	7.9	1.576	1.000	−25.83	−1.577	−0.996	25.82
6,2	105	7.9	1.580	1.000	−25.87	−1.581	−1.000	25.87
7,2	123	7.9	1.581	1.000	−25.87	−1.581	−1.000	25.87
8,2	141	7.8	1.581	1.000	−25.87	−1.581	−1.000	25.87
3,3	68	14.1	2.784	1.946	−46.29	−3.376	−1.577	51.71
4,3	92	2.3	1.685	1.132	−28.28	−1.741	−1.021	28.20
5,3	116	1.6	1.603	0.992	−25.92	−1.585	−1.026	25.92
6,3	140	1.3	1.603	0.993	−25.94	−1.586	−1.023	25.95
7,3	164	1.1	1.598	0.995	−25.93	−1.585	−1.016	25.93
8,3	188	1.0	1.593	0.997	−25.91	−1.584	−1.009	25.91

the first case Poisson's ratio (ν) is zero, in the second case $\nu = 0.3$ and plane strain conditions are assumed.

5.2.1. The case $\nu = 0$.

The results of computation are shown in Table 5.3. The errors for $p \leq 5$ are much larger than in the case of the moderately thick arch discussed in Section 5.1. Nevertheless, p-convergence is strong and at $p = 7, 8$ the equilibrium relations are satisfied to at least three digits of precision. Once again the data show that choice of the basis does not affect the accuracy of the solution significantly. For low p values the approximate solutions computed with curvilinear bases are worse than the approximate solutions computed with Cartesian bases. For high p values the curvilinear bases are slightly better, although both approaches yield good results.

Table 5.3. Circular arch, $r/t \approx 1000$, constant cross section, 3 elements, $\nu = 0$.

(a) Curvilinear basis.

p, q	N	$(e_r)_E$	F_{AX}	F_{AY}	M_{A0}	F_{BX}	F_{BY}	M_{B0}
3, 1	34	69.2	−54.812	−104.234	1763.79	131.438	−5.033	−1969.76
4, 1	46	9.7	−13.459	−26.267	440.09	28.010	−1.549	−417.16
5, 1	58	0.1	2.035	1.767	−40.27	−2.662	−0.981	42.90
6, 1	70	0.0	1.642	1.057	−28.10	−1.673	−0.999	28.07
7, 1	82	0.0	1.610	1.000	−27.11	−1.610	−1.000	27.11
8, 1	94	0.0	1.610	1.000	−27.12	−1.610	−1.000	27.12

(b) Cartesian basis.

p, q	N	$(e_r)_E$	F_{AX}	F_{AY}	M_{A0}	F_{BX}	F_{BY}	M_{B0}
3, 1	34	70.8	33.982	56.500	−988.73	−90.010	−0.664	1350.25
4, 1	46	11.2	16.860	30.957	−530.15	−39.502	0.903	594.98
5, 1	58	0.4	2.351	2.833	−56.49	−3.406	−0.761	54.06
6, 1	70	0.0	1.565	0.922	−25.77	−1.514	−0.998	25.68
7, 1	82	0.0	1.611	0.997	−27.09	−1.608	−1.000	27.09
8, 1	94	0.0	1.612	0.999	−27.12	−1.610	−1.000	27.12

The fully two dimensional solution, using the same three-element mesh, was computed by *PROBE*. At $p = 8$ the following stress resultants were obtained: $F_{AX} = 1.612$; $F_{AY} = 0.999$; $M_{A0} = -27.124$; $F_{BX} = -1.610$; $F_{BY} = -1.000$; $M_{B0} = -27.124$. The computed value of the strain energy at $p = 8$ $(N = 219)$ was $0.381787 \times 10^8/E$, where E is the modulus of elasticity.

5.2.2. The case $\nu = 0.3$, plane strain.

In the case of thin arches and shells Poisson's ratio does not affect the stress resultants significantly but it does affect the displacement and the strain energy. It also affects the discretization error in finite element computations. The approach presented herein provides for control of the discretization error. This is demonstrated in the following.

If we use the same three-element mesh as before, and $q = 2$, then we obtain the data shown in Table 5.4. We see that the error in stress resultants is large at the fixed support. The reason for this is that the radial displacement induced by the nonzero Poisson's ratio is prevented by the fixed support. This excites the singularities, causing an oscillatory behavior of the stresses in the element at the boundary. We refer to this as the *boundary layer effect.* To compensate for the boundary layer effect we need to introduce a small element which is approximately of the same size as the thickness of the arch or shell. The results obtained for a four element mesh, which differs from the mesh shown in Fig. 5.1 in that $r_i = 14.985$ and a fourth element of arc length 0.015 is introduced at the fixed boundary, is shown in Table 5.5. We see that there is a marked improvement in convergence and the stress resultants are converging to the same values as in the case of $\nu = 0$.

The fully two dimensional solution, using the same four-element mesh, was computed by *PROBE.* At $p = 8$ the following stress resultants were obtained: $F_{AX} = 1.610$; $F_{AY} = 1.000$; $M_{A0} = -27.125$; $F_{BX} = -1.611$; $F_{BY} = -1.000$; $M_{B0} = -27.128$. The computed value of the strain energy at $p = 8$ $(N = 295)$ was $0.347414 \times 10^8/E$ which is almost exactly $0.381787 \times 10^8\,(1-\nu^2)/E$, that is $(1-\nu^2)$ times the value of the strain energy computed for $\nu = 0$. Since the strain energy is proportional to the applied force times the displacement in the direction of the force, the displacements computed by the two methods are also close.

This example demonstrates that in the case of thin shells very good results can be obtained if we replace E with $E/(1-\nu^2)$ but otherwise use $\nu = 0$. If we do not use this simplification then we must take into consideration the boundary layer effects in designing the mesh and the value of q has to be at least 2.

5.3. Circular arch, variable cross section.

Our third example is the circular arch of variable cross section, shown in Fig. 5.2. The r/t ratio ranges from approximately 4 to approximately 15. The

Table 5.4. Circular arch, $r/t \approx 1000$, constant cross section, 3 elements, $\nu = 0.3$. Cartesian basis.

p, q	N	$(e_r)_E$	F_{AX}	F_{AY}	M_{A0}	F_{BX}	F_{BY}	M_{B0}
3, 2	51	72.0	40.540	70.051	−1213.92	−118.871	1.883	1782.86
4, 2	69	14.3	22.197	43.754	−736.68	−60.514	2.459	909.99
5, 2	87	8.0	0.145	0.875	−14.88	−5.073	−0.643	79.05
6, 2	105	6.7	−1.491	−2.574	42.22	−1.476	−0.997	25.11
7, 2	123	5.8	−1.525	−2.503	41.60	−1.614	−1.003	27.17
8, 2	141	5.1	−1.588	−2.522	42.35	−1.608	−0.998	27.09

Table 5.5. Circular arch, $r/t \approx 1000$, constant cross section, 4 elements, $\nu = 0.3$. Cartesian basis.

p, q	N	$(e_r)_E$	F_{AX}	F_{AY}	M_{A0}	F_{BX}	F_{BY}	M_{B0}
3, 2	69	71.7	−6.295	3.927	−6.16	−119.302	1.912	1789.32
4, 2	93	11.5	0.145	2.409	−34.54	−60.552	2.473	910.57
5, 2	117	0.8	0.633	1.557	−27.08	−5.051	−0.639	78.72
6, 2	141	0.6	1.155	1.264	−27.16	−1.480	−1.001	25.17
7, 2	165	0.6	1.418	1.111	−27.14	−1.606	−1.001	27.06
8, 2	189	0.6	1.537	1.043	−27.13	−1.611	−1.000	27.13
9, 2	213	0.6	1.584	1.015	−27.12	−1.611	−1.000	27.13
10, 2	237	0.6	1.602	1.005	−27.12	−1.611	−1.000	27.13

thickness is unity. To obtain reference values, the problem was solved as a problem of elasticity, by *PROBE* using 3 finite elements. The results are shown in Table 5.6. The estimated exact value of the strain energy, determined from a sequence of fully two dimensional solutions by *PROBE*, is $0.728440 \times 10^2/E$.

Table 5.6. Circular arch, variable cross section, 3 elements. Solution as a problem of elasticity.

p	N	$(e_r)_E$	F_{AX}	F_{AY}	M_A	F_{BX}	F_{BY}	M_B
1	10	86.8	0.734	1.512	−22.71	−0.394	−1.793	6.08
2	27	63.7	2.413	1.105	−32.15	−2.320	−3.431	34.22
3	44	22.7	1.694	1.164	−28.88	−3.547	−2.036	53.20
4	67	8.7	1.706	0.983	−26.79	−2.185	−0.990	33.89
5	96	4.5	1.714	1.000	−27.05	−1.715	−0.951	27.09
6	131	3.0	1.714	1.000	−27.04	−1.701	−0.996	26.86
7	172	2.3	1.714	1.000	−27.05	−1.712	−1.001	27.03
8	219	1.8	1.714	1.000	−27.05	−1.712	−1.001	27.03

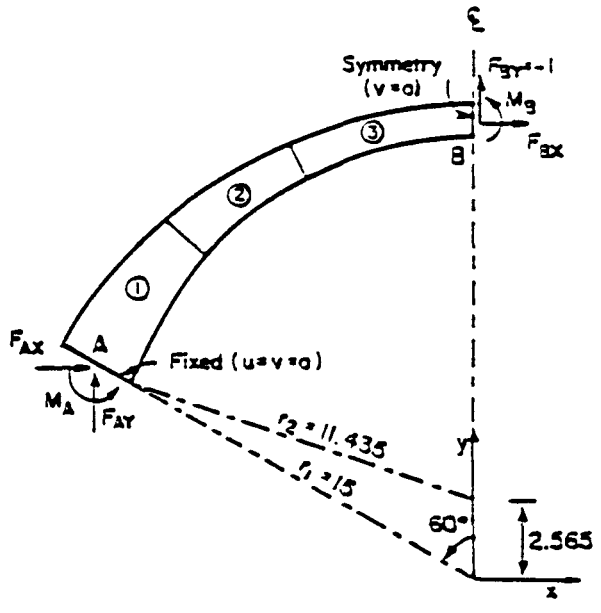

Fig. 5.2. Circular arch, variable cross section.

The results computed with the curvilinear and Cartesian bases are shown in Tables 5.7a, 5.7b. Although in this case the radius to thickness ratio is quite small, remarkably good results can be obtained with the lowest order approximation of the transverse displacement ($q = 1$). Compare, for example, the results obtained with the fully two-dimensional solution in Table 5.6, $p = 6$ and the results in Table 5.7b corresponding to $(p, q) = (6, 1)$.

For low q values the Cartesian basis is better, for high p values both approaches yield similarly good results. Once again, the error in energy norm is large for $q = 1, 2$ with a sharp decrease in the error at $q = 3$. This is due to better representation of the shear deformation terms at $q \geq 3$.

5.4. Cylindrical shell, r/t=100.

Our fourth example is one of the most widely investigated test problems in finite element analysis of shells, often called the *Scordelis-Lo problem* because the first finite element analysis of this problem was performed by Scordelis and Lo in 1964 [25]. Other finite element solutions were published by Cowper et al. [26] and Forsberg [27] in 1970; Dawe in 1975 [28]; MacNeal and Harder in

Table 5.7a. Circular arch, variable thickness, 3 elements. Curvilinear basis.

p, q	N	$(e_r)_E$	F_{AX}	F_{AY}	M_A	F_{BX}	F_{BY}	M_B
3, 1	34	26.0	1.559	1.081	−26.69	−1.209	−1.695	19.40
4, 1	46	23.2	1.733	1.032	−27.23	−1.606	−0.955	25.45
5, 1	58	23.2	1.710	1.010	−26.81	−1.711	−0.969	26.96
6, 1	70	23.2	1.711	1.016	−26.89	−1.710	−0.999	26.94
7, 1	82	23.2	1.711	1.015	−26.88	−1.706	−1.001	26.88
8, 1	94	23.2	1.711	1.015	−26.88	−1.706	−1.000	26.88
3, 2	51	15.3	1.512	1.072	−26.63	−1.195	−1.663	19.26
4, 2	69	10.1	1.729	1.014	−27.31	−1.614	−0.952	25.62
5, 2	87	10.1	1.708	0.992	−26.90	−1.719	−0.972	27.13
6, 2	105	10.0	1.712	1.000	−27.03	−1.717	−0.999	27.10
7, 2	123	10.0	1.713	1.000	−27.03	−1.713	−1.000	27.04
8, 2	141	10.0	1.713	1.000	−27.04	−1.713	−1.000	27.04
3, 3	68	12.2	1.539	1.062	−26.68	−1.189	−1.670	19.17
4, 3	92	2.7	1.740	1.010	−27.35	−1.613	−0.989	25.59
5, 3	116	2.1	1.715	0.989	−26.92	−1.719	−1.005	27.12
6, 3	140	1.8	1.716	0.999	−27.04	−1.717	−1.022	27.09
7, 3	164	1.7	1.715	0.999	−27.04	−1.714	−1.016	27.04
8, 3	188	1.5	1.713	1.000	−27.04	−1.713	−1.009	27.04
3, 4	85	12.2	1.538	1.062	−26.68	−1.189	−1.670	19.17
4, 4	115	2.6	1.739	1.009	−27.33	−1.613	−0.989	25.59
5, 4	145	1.9	1.713	0.988	−26.90	−1.719	−1.004	27.12
6, 4	175	1.6	1.713	0.998	−27.02	−1.717	−1.021	27.09
7, 4	205	1.4	1.713	0.999	−27.02	−1.714	−1.015	27.04
8, 4	235	1.3	1.712	1.000	−27.03	−1.713	−1.008	27.04

Table 5.7b. Circular arch, variable thickness, 3 elements.
Cartesian basis.

p, q	N	$(e_r)_E$	F_{AX}	F_{AY}	M_A	F_{BX}	F_{BY}	M_B
3, 1	34	19.7	1.736	1.428	−32.38	−3.274	−1.840	49.36
4, 1	46	11.4	1.682	0.952	−26.25	−2.037	−0.967	31.74
5, 1	58	11.1	1.716	1.000	−27.06	−1.707	−0.966	26.95
6, 1	70	11.1	1.713	1.001	−27.04	−1.705	−0.998	26.92
7, 1	82	11.1	1.713	1.000	−27.03	−1.712	−1.001	27.02
8, 1	94	11.1	1.713	1.000	−27.03	−1.713	−1.000	27.03
3, 2	51	19.1	1.726	1.424	−32.28	−3.276	−1.838	49.40
4, 2	69	10.2	1.675	0.946	−26.14	−2.036	−0.968	31.73
5, 2	87	9.9	1.712	0.998	−27.01	−1.707	−0.966	26.96
6, 2	105	9.9	1.711	0.999	−27.02	−1.705	−0.998	26.92
7, 2	123	9.8	1.712	1.000	−27.03	−1.712	−1.001	27.02
8, 2	141	9.8	1.713	1.000	−27.03	−1.713	−1.000	27.03
3, 3	68	16.8	1.760	1.418	−32.42	−3.297	−1.852	49.69
4, 3	92	3.3	1.689	0.944	−26.22	−2.047	−1.007	31.89
5, 3	116	1.9	1.722	0.997	−27.08	−1.716	−0.999	27.08
6, 3	140	1.6	1.717	1.000	−27.07	−1.713	−1.022	27.03
7, 3	164	1.4	1.715	1.000	−27.06	−1.719	−1.017	27.11
8, 3	188	1.3	1.714	1.000	−27.05	−1.718	−1.010	27.10
3, 4	85	16.8	1.759	1.418	−32.42	−3.297	−1.851	49.69
4, 4	115	3.2	1.688	0.944	−26.21	−2.047	−1.007	31.89
5, 4	145	1.7	1.719	0.997	−27.05	−1.716	−0.998	27.08
6, 4	175	1.4	1.715	0.999	−27.04	−1.713	−1.021	27.03
7, 4	205	1.2	1.713	0.999	−27.04	−1.719	−1.015	27.11
8, 4	235	1.0	1.713	1.000	−27.04	−1.718	−1.008	27.10

1985 [29], and Carpenter et al. in 1986 [30]. Displacement data, computed from solutions obtained with various finite element computer programs, are summarized in [31]. Both displacement data and stress resultants are given in [32]. Selected data computed from finite element solutions based on shallow shell formulation are tabulated in [26] and data computed from finite element solutions based on deep shell formulation are given in [28]. Reference data computed from the exact solution of the shallow shell formulation are given in [26].

5.4.1. Problem statement.

The shell is shown in Fig. 5.3. It is loaded by its own weight which is approximated by uniformly distributed traction of 90.0 lbf/ft^2 acting on the middle surface of the shell in the negative z direction. The cylindrical shell is supported by diaphragms at the ends. The diaphragms prevent displacement in the x and z directions but allow displacement in the y direction. Poisson's ratio is zero and the modulus of elasticity (E) is 3.0×10^6 lbf/in^2. Because there are two planes of symmetry, it is sufficient to discretize only one quarter of the shell. In the following we refer only to the domain ABCD, see Fig. 5.3. The goal of computation is to compute displacements, membrane forces and moments at selected points to about one percent relative error.

5.4.2. Solution as a problem in three dimensional elasticity.

The problem was solved as a problem in three dimensional elasticity by means of *PROBE*. Four finite elements mapped by quadratic parametric mapping were used. Half of the 90.0 lbf/ft^2 traction acting in the negative z direction was applied to the upper surface of the shell, half to the lower surface. The mesh and the deformed configuration are shown in Fig. 5.4. The computed values of the strain energy, the estimated relative error in energy norm $(e_r)_E$ and the displacement components $(u_x)_B$, $(u_y)_B$ are shown in Table 5.8.

The displacement component $(u_z)_B$ computed by various computer codes was plotted in [31] against N. The exact analytical solution reported for the shallow shell formulation is -3.70331 inches [26] and for the deep shell formulation is -3.53 inches [31]. Our three dimensional result of $(u_z)_B = -3.613$ inches agrees to at least three significant digits with the results obtained with *STARDYNE*'s *QUAD8*

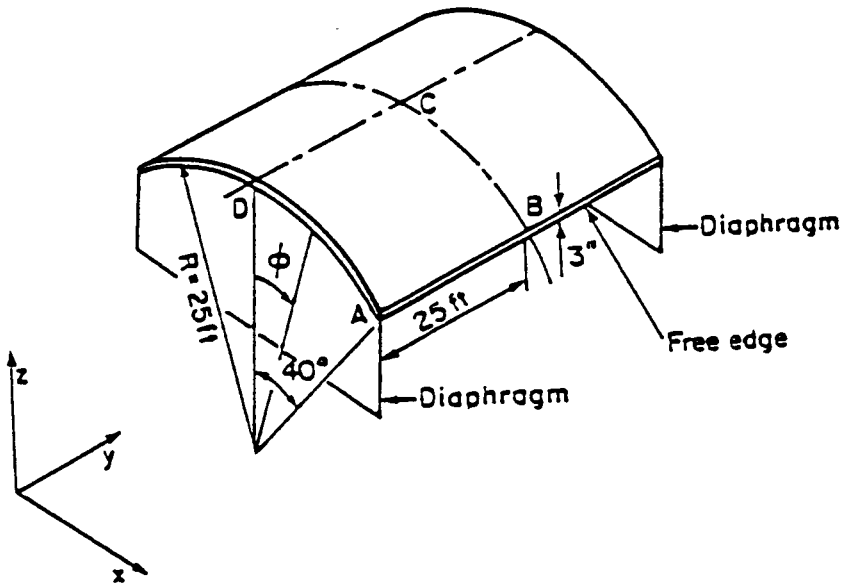

Fig. 5.3. Cylindrical shell problem. (Not to scale).

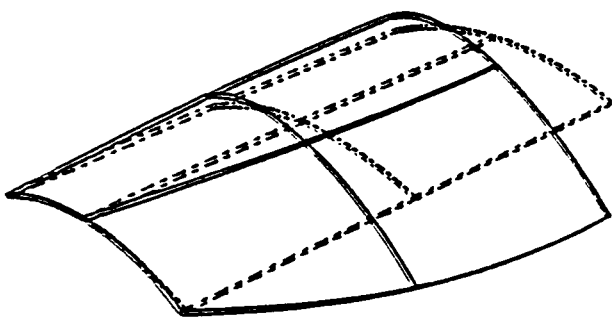

Fig. 5.4. Cylindrical shell. Deformed configuration. (Quarter model).

element using 2016 degrees of freedom and differ by less than one percent from the results obtained with *ABAQUS' S4R* element which yielded $(u_z)_B = -3.629$ inches when 2166 degrees of freedom were used [31]. The strain energy of the exact analytical solution of the shallow shell formulation is 0.14707×10^5 in $\cdot$ lbf for one quarter of the shell [26]. Of course, the exact solution of the three dimensional formulation is not known. Our estimate of the exact value of the strain energy corresponding to the three dimensional formulation is 0.145049×10^5 in $\cdot$ lbf. This

Table 5.8. Computed values of the strain energy, estimated relative error $e_r(\vec{u}_{FE})$ (percent) and displacement components $(u_x)_B$, $(u_y)_B$. Solution as a problem in three dimensional elasticity. Four finite elements.

p	N	$U(\vec{u}_{FE})$ (in · lbf)	$e_r(\vec{u}_{FE})$	$(u_x)_B$ (in)	$(u_y)_B$ (in)
1	32	0.942193×10^3	96.69	−0.081	−0.003
2	104	0.605197×10^4	76.34	−0.937	−0.360
3	176	0.120684×10^5	40.98	−2.927	−1.525
4	300	0.144160×10^5	7.83	−3.606	−1.902
5	476	0.144844×10^5	3.76	−3.611	−1.903
6	716	0.144896×10^5	3.25	−3.611	−1.903
7	1032	0.144924×10^5	2.94	−3.612	−1.903
8	1436	0.144950×10^5	2.61	−3.613	−1.904

value was found by extrapolation based on detailed analyses. The relative errors were computed with reference to this value.

5.4.3. Solution by hierarchic shell model, Cartesian basis, $q = 1$.

In the hierarchic model mapping was by the blending function method. Uniformly distributed tractions were applied on the upper and lower surfaces of the shell so that the total force acting on the upper surface was the same as the total force acting on the lower surface. The strain energy, the estimated relative error in energy norm $e_r(\vec{u}_{FE})$, and the displacement components $(u_x)_B$, $(u_y)_B$ computed from solutions obtained by means of the hierarchic shell model, Cartesian basis, $q = 1$ with one finite element (resp. four finite elements) are given in Table 5.9a (resp. Table 5.9b). On comparing the results in Tables 5.9a,b with those in Table 5.8, we see that the simplest hierarchic shell model yields results which are of similar quality as the results obtained with the fully three dimensional model when $\nu = 0$. The strain energy of the fully three dimensional model at $p = 8$, $N = 1436$ is slightly lower than the strain energy of the hierarchic shell model, Table 5.9b, $(p, q) = 8, 1$. This result appears to be inconsistent because the finite element meshes are the same and $\mathcal{S}^{8,1}$ is a subset of the standard polynomial space in *PROBE* corresponding to $p = 8$. In reality there is no inconsistency, however: The finite element space defined by the shell model is not a subset of the finite element space defined by the fully three dimensional model. This is because in the fully three dimensional model quadratic parametric mapping was used whereas in the hierarchic shell model mapping was by the blending function method so that

Table 5.9a. Computed values of the strain energy, estimated relative error $e_r(\vec{u}_{FE})$ (percent) and displacement components $(u_z)_B$, $(u_x)_B$. Solution by hierarchic shell model. Cartesian basis. One finite element.

p, q	N	$U(\vec{u}_{FE})$ (in · lbf)	$e_r(\vec{u}_{FE})$	$(u_z)_B$ (in)	$(u_x)_B$ (in)
4, 1	64	0.856464×10^4	63.99	−1.799	−8.730
6, 1	126	0.144514×10^5	6.07	−3.623	−1.912
8, 1	212	0.144881×10^5	3.40	−3.610	−1.903
10, 1	322	0.144924×10^5	2.94	−3.612	−1.904
12, 1	456	0.144957×10^5	2.52	−3.613	−1.904

Table 5.9b. Computed values of the strain energy, estimated relative error $e_r(\vec{u}_{FE})$ (percent) and displacement components $(u_z)_B$, $(u_x)_B$. Solution by hierarchic shell model. Cartesian basis. Four finite elements.

p, q	N	$U(\vec{u}_{FE})$ (in · lbf)	$e_r(\vec{u}_{FE})$	$(u_z)_B$ (in)	$(u_x)_B$ (in)
4, 1	224	0.144130×10^5	7.96	−3.606	−1.902
6, 1	456	0.144903×10^5	3.17	−3.611	−1.903
8, 1	784	0.144952×10^5	2.58	−3.613	−1.904
10, 1	1208	0.144993×10^5	1.96	−3.615	−1.905
12, 1	1728	0.145022×10^5	1.36	−3.616	−1.906

Table 5.10a. Displacement, moment and membrane force data at points B and C. Solution by hierarchic shell model. Cartesian basis. One finite element.

p, q	N	$(u_z)_C$ (in)	$(N_\phi)_C$ (lbf/in)	$(N_y)_C$ (lbf/in)	$(M_y)_C$ (lbf)	$(M_\phi)_C$ (lbf)	$(N_y)_B$ (lbf/in)	$(M_y)_B$ (lbf)
4, 1	64	0.0668	−4088.2	10778.0	169.4	1120	4700	−539.9
6, 1	126	0.5353	−15325.0	−72.4	61.2	1951	6408	−642.2
8, 1	212	0.5422	−304.9	−117.8	104.4	2088	6328	−634.8
10, 1	322	0.5417	−297.7	−130.8	101.5	2060	6306	−644.3
12, 1	456	0.5412	−285.9	−133.4	97.1	2058	6313	−643.7

Table 5.10b. Displacement, moment and membrane force data at points B and C. Solution by hierarchic shell model. Cartesian basis. Four finite elements.

p, q	N	$(u_z)_C$ (in)	$(N_\phi)_C$ (lbf/in)	$(N_y)_C$ (lbf/in)	$(M_y)_C$ (lbf)	$(M_\phi)_C$ (lbf)	$(N_y)_B$ (lbf/in)	$(M_y)_B$ (lbf)
4, 1	224	0.5363	39276.0	922.4	150.3	2108	9420	−704.5
6, 1	456	0.5415	−2157.1	−134.5	94.0	2055	6318	−645.4
8, 1	784	0.5418	−283.8	−133.2	95.8	2059	6312	−643.6
10, 1	1208	0.5420	−285.5	−132.7	95.8	2059	6314	−642.3
12, 1	1728	0.5422	−283.7	−132.5	95.9	2059	6314	−641.5

the cylindrical surfaces were exactly represented. In addition, there were slight differences in loading: In the three dimensional model half of the traction was applied to the upper surface, half to the lower surface of the shell. In the hierarchic shell model the traction of 90 lbf/ft^2 was split between the upper and lower surfaces so that the force acting on the upper surface was equal to the force acting on the lower surface.

Additional data are presented in Tables 5.10a,b. The definitions of N_ϕ, N_y, M_ϕ, M_y are as follows: N_ϕ and M_z are defined on sections of constant ϕ, see Fig. 5.3:

$$N_\phi \stackrel{\text{def}}{=} \int_{r_i}^{r_o} \sigma_\phi \, dr, \qquad M_\phi \stackrel{\text{def}}{=} \int_{r_i}^{r_o} \sigma_\phi \, (r - r_m) \, dr \tag{5.3a}$$

where σ_ϕ is the normal stress in the r, ϕ, y system; r_i (resp. r_o) is the inner (resp. outer) radius of the shell and $r_m \stackrel{\text{def}}{=} (r_i + r_o)/2$ is the mean radius. Similarly N_y and M_y are defined on sections of constant y:

$$N_y \stackrel{\text{def}}{=} \int_{r_i}^{r_o} \sigma_y \, dr, \qquad M_y \stackrel{\text{def}}{=} \int_{r_i}^{r_o} \sigma_y \, (r - r_m) \, dr. \tag{5.3b}$$

Convergence of the tabulated data is evident. When convergence is monotonic then some simple extrapolation scheme may be used to estimate limiting values. When convergence is oscillatory then the average of consecutive data is generally a good estimate of the limiting value.

6. SUMMARY AND CONCLUSIONS.

The only means for ensuring and verifying that engineering data computed from finite element solutions are within acceptable tolerance levels is by performing extensions. Extensions are orderly sequences of discretization constructed in such a way that the sequence of finite element solutions corresponding to a sequence of discretization converges to the exact solution. Of course, the exact solution and the norms in which convergence can be meaningfully measured depend on the choice of generalized formulation. In this paper the generalized formulation considered is the principle of virtual work.

In conventional theories for curved beams, arches and shells the generalized formulation, as well as the displacement modes and stress distributions, vary from theory to theory. For this reason conventional theories do not constitute an orderly sequence, so that the corresponding solutions converge to the exact solution of a particular generalized formulation.

In this paper we proposed an orderly sequence of discretizations controlled by two parameters. One of the parameters, denoted by p, represents the polynomial degree of basis functions with respect to standard coordinates mapped to the middle surface. The other parameter, denoted by q, represents the polynomial degree of the basis functions with respect to the standard coordinates which is mapped transversely to the middle surface. The finite element solutions converge to the exact solution of the fully three dimensional formulation of the theory of elasticity, based on the principle of virtual work, as $p \rightarrow \infty$ and $q \rightarrow \infty$. The examples presented herein are representative of a large class of problems which include thick, moderately thick and thin arches and shells. The results show that coarse meshes and $q = 1$, $5 \leq p \leq 12$, are generally sufficient to achieve levels of accuracy in the computed displacements, shear forces and moments which are normally expected in engineering practice. The hierarchic model characterized by $q = 1$ is similar to the Reissner-Mindlin theory except that one additional field which represents linear variation of the transverse displacement is incorporated.

The modeling strategy outlined herein views any beam, arch, plate or shell model as a particular discretization of the fully three dimensional model. Given a fixed finite element mesh, p-extension is performed when either p or q is increased. Convergence to the exact three dimensional solution is guaranteed. Recent surveys of the theoretical basis of p-extensions are available in [33,34]. The efficiency of p-extensions depends on the finite element element mesh. Initial mesh design is based on the analyst's judgement concerning the expected smoothness of the solution. Modification of the initial mesh design is based on information generated by p-extension [24].

Our investigation has shown that curvilinear bases are not more advantageous than Cartesian bases in computer implementations. Originally, curvilinear bases had been used to permit analytical solutions for cylindrical, spherical, conical, toroidal and other shells mapped by relatively simple functions. In problems of current computer aided design and analysis a much wider range of mapping functions must be considered. Also, shells are connected to attachment lugs, stiffeners, etc. and are joined with other shells. In such regions the assumptions of conventional shell theories do not hold, and analytical treatment is impossible, yet those are the regions which are of greatest practical interest. The use of Cartesian bases provides for connection of shells of various types, stiffeners, three dimensional elements, etc., in a natural and systematic way. There is no need for transition elements and the process is computationally efficient.

We have defined hierarchic sequences of basis functions based on Legendre polynomials. These basis functions lead to well conditioned stiffness matrices so that the accumulation of round-off error with respect to increasing p is slow. We have not encountered problems caused by round-off even at extreme aspect ratios (see Section 5.2) and $p = 12$.

We have demonstrated by an example that in the case of thin arches and shells finite element discretizations can be substantially simplified by replacing E with $E/(1-\nu^2)$ but otherwise using $\nu = 0$. The computed values of the stress resultants and displacements are not affected significantly by this substitution.

7. REFERENCES

[1] Naghdi, P. M., "The Theory of Shells and Plates" *Handbuch der Physik*, Vol. VIa/2, pp. 425-640, Springer-Verlag, Berlin (1972).

[2] Naghdi, P. M., "On the Theory of Thin Elastic Shells", *Quarterly of Applied Mathematics*, Vol. XIV, No. 4, pp. 369-380 (1957).

[3] Timoshenko, S. and Woinowsky-Krieger, S., *Theory of Plates and Shells*, 2nd Ed., McGraw-Hill (1959).

[4] Novozhilov, V. V., *Thin Shell Theory*, 2nd English translation, P. Noordhoff Ltd., Groningen (1964).

[5] Goldenveizer, A. L., "Derivation of an Approximate Theory of Bending of a Plate by the Method of Asymptotic Integration of the Equations of the Theory of Elasticity", *Prikl. Mat. Mech.*, Vol. 26, pp. 668-686 (1962). English translation: P.M.M., pp. 1000-1025 (1964).

[6] Goldenveizer, A. L., "The Principles of Reducing Three-dimensional Problems of Elasticity to Two-Dimensional Problems of the Theory of Plates and Shells", *Proc. 11th International Congress of Theoretical and Applied Mechanics*, H. Gortler, Ed., Springer Verlag, Munich, pp. 306-311, (1964).

[7] Frederichs, K. O. and Dressler, R. F., "A Boundary-Layer Theory for Elastic Plates" *Comm. Pure Appl. Math.*, Vol. 14, pp. 1-33 (1961).

[8] Reiss, E. L. and Locke, S., "On the Theory of Plane Stress" *Quart. Appl. Math.*, Vol. 19, pp. 195-203 (1961).

[9] Ciarlet, P. G. and Destuynder, P., "A Justification of the Two-dimensional Linear Plate Model", *Journal de Mèchanique*, Vol. 18, pp. 315-343 (1979).

[10] Antman, S. S., "The Theory of Rods", *Handbuch der Physik*, Vol. VIa/2, pp. 641-703, Springer-Verlag, Berlin (1972).

[11] Kirchhoff, G., "Über das Gleichgewicht und die Bewegung einer elastischen Scheibe" *Crelles J.*, Vol 40, pp. 51-88 (1850).

[12] Love, A. E. H., "The Small Free Vibrations and Deformation of Thin Elastic Shells", *Phil. Trans. Royal Soc.*, London, Ser. A, Vol. 181, pp. 491-546 (1886).

[13] Reissner, E., "On the Theory of Bending of Plates", *J. Math. Phys.*, Vol. 23, pp. 184-191 (1944).

[14] Reissner, E., "The Effects of Transverse Shear Deformation on the Bending of Elastic Plates", *J. Appl. Mech., Trans. ASME*, Vol. 67, pp. 69-77 (1945).

[15] Mindlin, R. D., "Influence of Rotatory Inertia and Shear on Flexural Motions of Isotropic, Elastic Plates", *J. Appl. Mech., Trans. ASME*, Vol. 73, pp. 31-38 (1951).

[16] Reissner, E., "Stress-Strain Relations in the Theory of Thin Elastic Shells" *J. Math. Phys.*, Vol. 31, pp. 109-199 (1952).

[17] Lo, K. H., Christensen, R. M. and Wu, E. M., "A High-Order Theory of Plate Deformation - Part 1: Homogeneous Plates", *Journal of Applied Mechanics*" ASME, Vol. 44, pp. 663-668 (1977).

[18] Lo, K. H., Christensen, R. M. and Wu, E. M., "A High-Order Theory of Plate Deformation - Part 2: Laminated Plates", *Journal of Applied Mechanics*" ASME, Vol. 44, pp. 669-676 (1977).

[19] Rossow, M. P. and Katz, I. N., "Hierarchal Finite Elements and Precomputed Arrays", *Int. J. num. Meth. Engng.*, Vol. 12, pp. 977-999 (1978).

[20] Rossow, M. P. and Chen, K. C., "Computational Efficiency of Plate Elements", Technical Note, *J. Struct. Div., ASCE*, Vol. 103, No. ST2, pp. 447-451 (1977).

[21] Szabó, B. A., *PROBE: Theoretical Manual*, Noetic Technologies Corp., St. Louis, Missouri (1985)

[22] Szabó, B. A., "Design of Finite Element Software for Reliability and Robustness", *Proc., Int.'l Conf. on Reliability and Robustness of Engineering Software, Como, Italy* 23-25 Sept., 1987

[23] Szabó, B., "Estimation and Control of Error Based on P-Convergence" in: I. Babuška, J. Gago, E. R. de A. Oliveira and O. C. Zienkiewicz, editors, *Accuracy Estimates and Adaptive Refinements in Finite Element Computations*, John Wiley & Sons Ltd., pp. 61-78 (1986).

[24] Szabó, B. A., "Mesh Design for the p-Version of the Finite Element Method", *Computer Methods in Applied Mechanics and Engineering*, Vol. 55, pp. 181-197 (1986).

[25] Scordelis, A. C. and Lo, K. S., "Computer Analysis of Cylindrical Shells", *J. Am. Concr. Inst.*, Vol. 61, pp. 539-561 (1964).

[26] Cowper, G. R., Lindberg, G. M. and Olson, M. D., "A Shallow Shell Finite Element of Triangular Shape", *Int. J. Solids Structures*, Vol. 6, pp. 1133-1156 (1970).

[27] Forsberg, K., "An Evaluation of Finite Difference and Finite Element Techniques for Analysis of General Shells", *Proc. IUTAM Symposium*,, Edited by B. Fraeijs de Veubeke, Université de Liège, Vol. 2, 837-858 (1970).

[28] Dawe, D. J., "Higher-Order Triangular Finite Element for Shell Analysis", *Int. J. Solids Structures*, Vol. 1, pp. 1097-1110 (1975)

[29] MacNeal, R. H. and Harder, R. L., "A Proposed Standard Set of Problems to Test Finite Element Accuracy," *Finite Elements in Analysis and Design*, Vol. 1, pp. 3-20 (1985).

[30] Carpenter, N., Stolarski, H. and Belytschko, T., "Improvements in 3-Node Triangular Shell Elements", *Int. J. num. Meth. Engng.*, Vol. 23, pp. 1643-1667 (1986).

[31] Fong, H., "Eight US General Purpose FE Programs", *Structural Mechanics Software Series*, Vol. 5, Edited by N. Perrone, W. Pilkey, and B. Pilkey, University Press of Virginia, Charlottesville, VA, pp. 125-156, (1984).

[32] Zienkiewicz, O. C., *The Finite Element Method*, McGraw-Hill Book Company (UK) Ltd. (1977).

[33] Babuška, I., "The p- and hp-Versions of The Finite Element Method. The State of the Art", *Finite Elements: Theory and Application*, edited by D. L. Dwoyer, M. Y. Hussaini and R. G. Voigt, Springer (1988).

[34] Suri, M., "The *p*-Version of the Finite Element Method for Elliptic Problems", *Advances in Computer Methods for Partial Differential Equations*, Vol. VI, Edited by R. Vichnevetsky and R. S. Stepleman, IMACS, pp. 85-91 (1987).

NASA
National Aeronautics and Space Administration

Report Documentation Page

1. Report No.	2. Government Accession No.	3. Recipient's Catalog No.
NASA CR-4203		

4. Title and Subtitle
Hierarchic Plate and Shell Models Based on p-Extension

5. Report Date
December 1988

6. Performing Organization Code

7. Author(s)
Barna A. Szabó and Glenn J. Sahrmann

8. Performing Organization Report No.
WU/CCM-87/5

9. Performing Organization Name and Address
Washington University
Center for Computational Mechanics
Campus Box 1129
One Brookings Drive
St. Louis, Missouri 63130

10. Work Unit No.
505-63-01-10

11. Contract or Grant No.
NAG1-639

12. Sponsoring Agency Name and Address
National Aeronautics and Space Administration
Langley Research Center
Hampton, VA 23665-5225

13. Type of Report and Period Covered
Contractor Report

14. Sponsoring Agency Code

15. Supplementary Notes
NASA Langley Research Center Technical Monitor: Norman F. Knight, Jr.

A summary of the work reported herein was presented at a conference at which Professor Babuška was honored for his numerous contributions in the fields of engineering and applied mathematics. The conference, entitled: "The Impact of Mathematical Analysis on the Numerical Solution of Engineering Problems", was held at the University of Maryland, College Park, MD September 17 - 19, 1986.

16. Abstract

This paper is concerned with formulations of finite element models for beams, arches, plates and shells based on the principle of virtual work. The focus is on computer implementation of hierarchic sequences of finite element models suitable for numerical solution of a large variety of practical problems which may concurrently contain thin and thick plates and shells, stiffeners, and regions where three dimensional representation is required. The approximate solutions corresponding to the hierarchic sequence of models converge to the exact solution of the fully three dimensional model. The stopping criterion is based on (1) estimation of the relative error in energy norm; (2) equilibrium tests, and (3) observation of the convergence of quantities of interest.

17. Key Words (Suggested by Authors(s))	18. Distribution Statement
Structural beams arches, plates, shells, numerical analysis, finite element methods, p-extensions, error estimate, hierarchic basis functions.	Unclassified—Unlimited Subject Category 39

19. Security Classif.(of this report)	20. Security Classif.(of this page)	21. No. of Pages	22. Price
Unclassified	Unclassified	48	A03

For sale by the National Technical Information Service, Springfield, Virginia 22161-2171